DOI: 10.53469/jpce.2025.07(01).06

Study on Shear Characteristics and Ultimate Bearing Capacity of Calcareous Silt Solidified by Fluorogypsum-Slag-Based Binders

Tengqin Cheng, Wenting Dai*, Renchao Zhang, Yunxiao Liu

College of Construction Engineering, Jilin University, Changchun, Jilin, China
Correspondence Author: daiwt@jlu.edu.cn

Abstract: ***Calcareous silt exhibits a higher concentration of calcium carbonate. Due to its inherently inferior engineering properties, calcareous silt necessitates solidification treatment prior to utilization. The shear strength of calcareous silt serves as a pivotal metric for evaluating the calcareous silt's capacity to withstand shear deformation, which is of paramount importance for assessing soil stability and engineering performance. To explore the engineering properties of calcareous silt solidified with a fluorgypsum-slag-based(F) binders, this research utilized such an agent to solidify calcareous silt. Direct shear tests were subsequently conducted on the solidified calcareous silt samples to analyze the shear behavior of the silt at varying curing durations and solidifying agent dosages. numerical simulations of the ultimate bearing capacity of foundations were carried out using the Abaqus numerical modeling software. The experimental findings reveal that the F group possesses superior shear characteristics compared to cement group, with a 28-day cohesion value of 1365.36 KPa and a friction angle of 39.62° for the F20 cohort. The F group exhibits a tendency towards brittle failure influenced by aging and dosage, whereas the cement group demonstrates plastic failure traits. The rate of cohesion enhancement in the F group diminishes with aging but escalates with increased dosage. Numerical simulations indicate that the F group exhibits a notably higher ultimate bearing capacity of 5460.75 KPa, underscoring its excellent engineering efficacy.***

Keywords: Calcareous silt, Shear performance, Abaqus, Ultimate bearing capacity of foundation.

1. Introduction

In the process of urbanization, the construction of underground projects and harbor facilities generates a significant amount of waste mud [1]. Improper disposal of this mud can lead to the encroachment of land resources, cause environmental pollution, and pose safety hazards [2]. calcareous silt is a type of silt with a high content of calcium carbonate [3]. Currently, research on silt solidification primarily focuses on siliceous-aluminous silt, with relatively few studies on the engineering properties of solidified calcareous silt [4]. The resourceful utilization of silt represents a primary approach to achieving green construction in engineering projects. By solidifying silt into soil suitable for engineering purposes, it becomes feasible to effectively utilize silt [5]. Traditionally, cement has been employed for the solidification of silt [6]; however, this method encounters issues such as low strength and high cement demand. Furthermore, cement production entails resource consumption and environmental pollution [7]. The utilization of solid waste as a partial substitute for cement to formulate a solid waste-based solidifying agent can overcome the deficiencies associated with cement-solidified silt [8]. This approach holds significant importance in realizing the resourceful utilization of industrial waste residues and silt, and in embodying the environmental protection principle of efficient waste utilization [9].

Fluorogypsum, a by-product of hydrogen fluoride production from sulfuric acid and fluorite, resembles natural anhydrite in composition [10]. Slag and fly ash, by-products of blast furnace ironmaking and coal combustion in thermal power plants respectively, exhibit high pozzolanic activity and hold potential for soil stabilization applications [11]. Calcium carbide residue is the solid waste produced after the hydrolysis of calcium carbide to produce acetylene, which belongs to industrial solid waste and accumulates in large quantities [12].

Extensive scholarly research has been dedicated to the investigation of silt solidification processes., Pan conducted research on river sediment, utilizing a series of experiments, including unconfined compressive strength tests, microscopic imaging, and phase analysis (such as SEM and XRD), to evaluate the effectiveness of stabilizers at different mixing ratios and curing ages. The results indicated that by optimizing the stabilizer formulation, the strength of river sediment could be effectively enhanced, and the leaching of heavy metals could be reduced [13]. Wang used the SICP method to solidify Yellow River sediment, aiming to improve its mechanical properties. Results showed significant enhancements in both mechanical properties and $CaCO_3$ content, with a linear relationship between UCS and $CaCO_3$ content. The $CaCO_3$, in the form of calcite, adhered to particle surfaces and filled interparticle pores, enhancing cohesion while maintaining permeability [14]. Hou explored the use of sodium silicate-activated slag/fly ash to solidify soft soil in the coastal regions of southern China. He discovered that the addition of sodium silicate had a significant impact on the strength of the solidified soil. As the content of sodium silicate increased, the strength of the solidified soil gradually rose, indicating that sodium silicate could activate the latent reactivity of the solidifying agent. Notably, the maximum strength of the sodium silicate-activated slag solidified soil reached 850 kPa, which was 155% higher than that of the soil solidified with slag alone [15].

there is limited research on the solidification of calcareous silt. This paper aims to explore the shear properties of calcareous silt solidified with fluorogypsum-based binders through direct shear tests. Furthermore, the ultimate bearing capacity of the solidified calcareous silt, when utilized as foundation fill, will

be analyzed using Abaqus simulation software. The objective is to investigate the potential for resource utilization of calcareous silt and to assess the mechanical properties of fluorgypsum-slag-based binders.

2. Materials and Methods

2.1 Raw Material Properties

1) calcareous silt

The calcareous silt was taken from Yichang, black in color and fluid-plastic. The basic physical property was shown in Table 1, and the particle size distribution as shown in Figure 1. calcareous silt was dried and pulverized at low temperature (50℃), and deionized water (w=55%) was added, stirred well, and settled for 24 hours, which was used as the soil for the test. The main components of the l calcareous silt used in the experiment, measured through X-ray diffraction (XRD), are shown in Figure 2. The silt contains quartz, calcite, kaolinite, muscovite, clinochlore and other components, with the primary mineral phases being calcite, quartz, kaolinite, and muscovite.

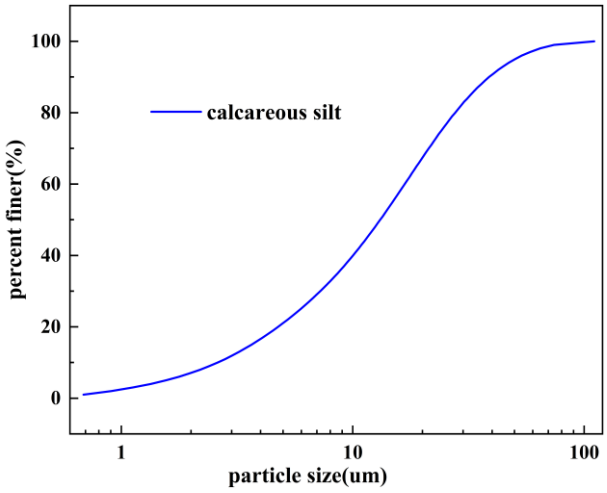

Figure 1: Grain size distribution

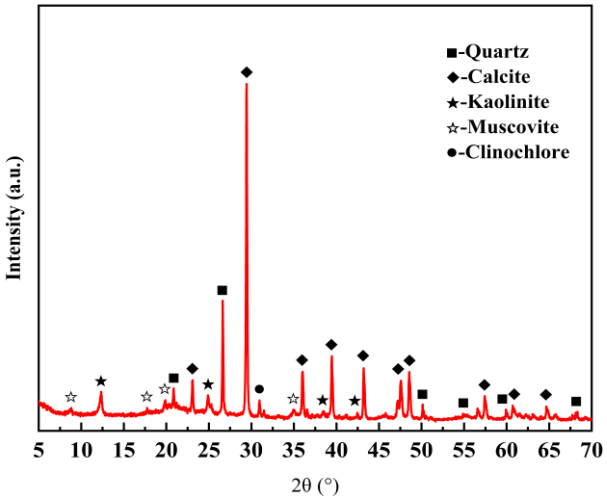

Figure 2: XRD results of calcareous silt

2) cement

Portland cement is P.O42.5 cement purchased from Yangchun Cement Co., Ltd. located in Zhucheng City. Specific surface area: 368 m²/g; initial setting time: 184 min; final setting time: 265 min.

3) slag

slag is S105 grade slag micro powder purchased from Longze Water Purification Materials Co. The specific surface area of the slag was 628 square meters per kilogram and the flowability ratio was 102%. The slag has a 7d activity index of 98% and a 28d activity index of 115%.

4) fly ash

Fly ash was produced by Wuhu Environmental Protection Technology Co., Ltd. in Henan Province.

5) fluorine gypsum

fluorine gypsum was produced by Xingsheng Calcium Co., Ltd. in Henan Province.

6) calcium carbide slag

calcium carbide slag was produced by Wuhu Environmental Protection Technology Co.

Table 1: Basic properties of calcareous silt

G_S	W_L	W_P	e	I_P	specific gravity (g/cm³)
2.68	20.4	37.1	1.5	22.9	1.45

2.2 Specimen Preparation

Calcareous silt will be dried and ground over 2mm sieve, and then the dried calcareous silt and curing agent with water for mixing, the water content to 55%, this paper sets 10%, 15%, 20% of three groups of proportion, pouring to make a specimen. Specimens, vibration with vibration table vibration, and covered with plastic wrap for 24h, and then demolded and curing to the specified age. To assess the impact of fluorgypsum-slag-based solidifying agent on calcareous silt performance, a cement control group was established. The solidifying agent is detailed in Table 2.

Table 2: Proportion of components in different binders

	cement	GGBS	Flyash	fluorogypsum	CCR
F	30	34.5	11.5	14	10
PO	100	0	0	0	0

2.3 Experimental Methods

The direct shear strength test was conducted by automatic four-connected direct shear apparatus, and the test was carried out at the specified age, with the axial stress controlled at 50, 100, 200 and 300 KPa. The specific proportions of the solidified calcareous silt and the experimental scheme are outlined in Table 3.

Table 3: Test scheme of solidified calcareous silt

bonder	proportion	water content	Curing day/d
F	10	1: 0.55	7,14,28d
F	15		
F	20		
PO	10		

3. Experimental Results and Discussion

3.1 Stress-strain Behavior

As shown in Figure 3, at 7-day curing age, the shear stress-shear displacement curves for both the 10% Fluorogypsum-Slag-Based (F) group and the cement group exhibit relative smoothness, indicating a stable shear deformation process. A slight decrease after reaching the peak and a relatively smooth stress-strain curve are observed. As the F content increases to 15% and 20%, the curves demonstrate distinct brittle failure characteristics, specifically characterized by a rapid rise to a peak followed by a sharp decline. This is attributed to the higher F content promoting the formation of more cementitious materials and ettringite, significantly enhancing the connections [16] between calcareous silt particles, improving the integrity and strength of the calcareous silt, and absorbing more free water, leading to brittle behavior similar to rock in the calcareous silt. The 10% F group displays clear peaks under all tested confining pressures. For the cement group, the curves are smooth and exhibit obvious plastic characteristics at higher confining pressures (200 kPa and 400 kPa), but similar peak failure as observed in the 10% fluorogypsum-blended group occurs at lower confining pressures (50 kPa and 100 kPa). The increase in F content significantly alters the shear behavior of solidified silt at 7 days, increasing soil brittleness. The mechanical response of cement-solidified calcareous silt varies with confining pressure.

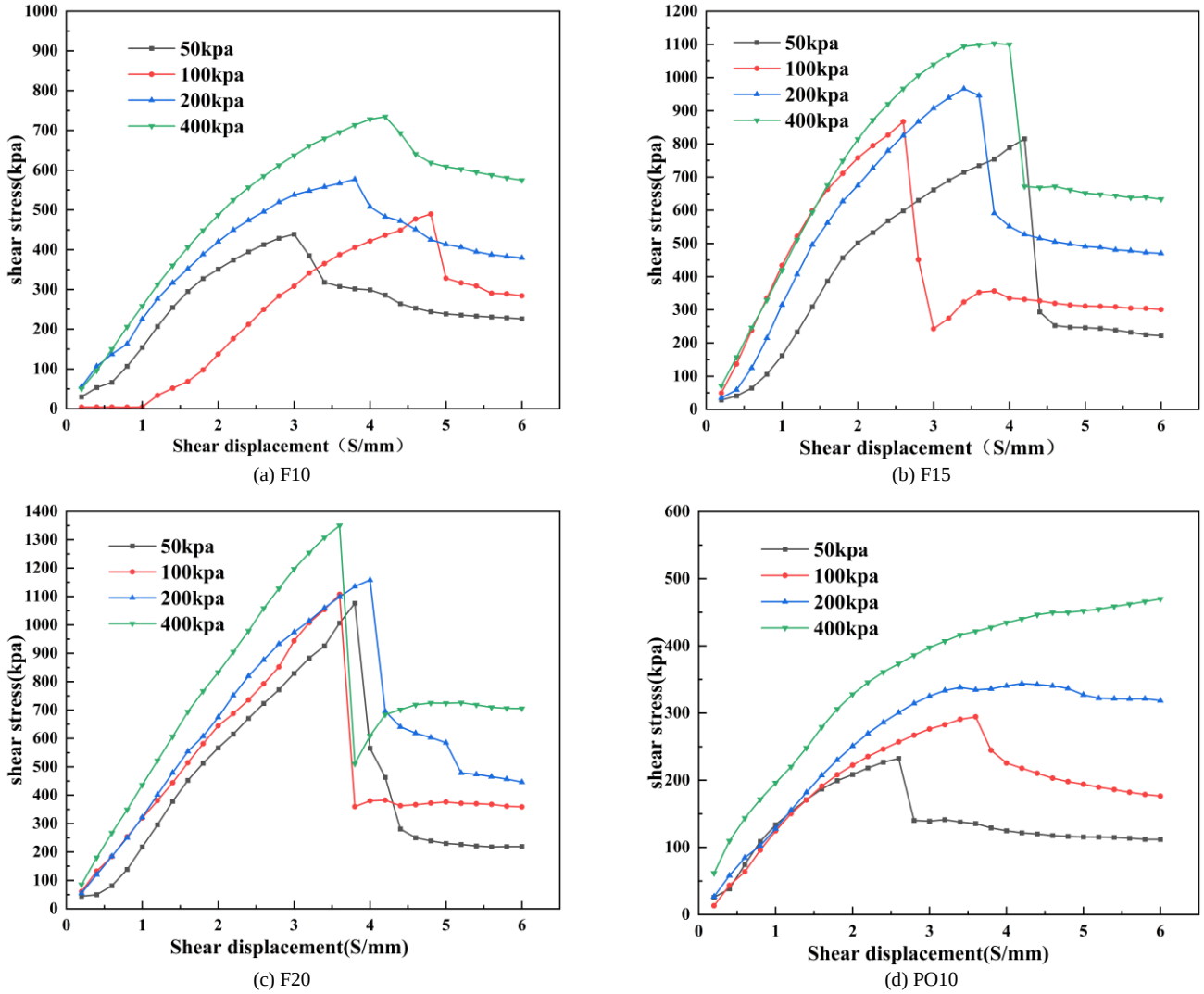

(a) F10 (b) F15

(c) F20 (d) PO10

Figure 3: Shear stress-strain curve for solidified calcareous silt at 7-day curing age (a)F10, (b)F15, (c)F20, (d)PO10

As illustrated in Figure 4, the 10% Fluorogypsum-Slag-Based (F) group at a 14-day curing age also exhibits partial brittle failure characteristics with fracturing under a low confining pressure of 50 kPa. Overall, compared to the 7-day curing age, there is an increase in stress-strain curves displaying brittle failure characteristics with fracturing, and the rate of rapid descent becomes more pronounced. The stress-strain characteristics of the cement group remain similar to those at the 7-day curing age. Meanwhile, there is a notable increase in the peak stress-strain values for all groups under various confining pressures. This may be due to the continued hydration reaction in the F group as the curing age increases. During this process, more cementitious materials and ettringite are formed, thereby enhancing the connections between soil particles and improving the integrity and strength of the soil mass. This reinforcement leads to the transformation of stress-strain curves into brittle failure characteristics in some cases, as evidenced by the rapid descent of the curves after reaching their peaks. This indicates that with the increase in curing age and the progression of the hydration reaction, the mechanical properties of the Fluorogypsum-Slag-Based solidified silt gradually tend to

enhance, accompanied by an increase in brittleness. The mechanical properties of the cement group also increase with the curing age; however, the cement group still exhibits obvious plastic characteristics at the 14-day curing age. Its stress-strain curves are smooth, with a gradual increase in stress, reflecting the gradual stabilization and strengthening of the internal structure of cement-solidified silt during the aging process.

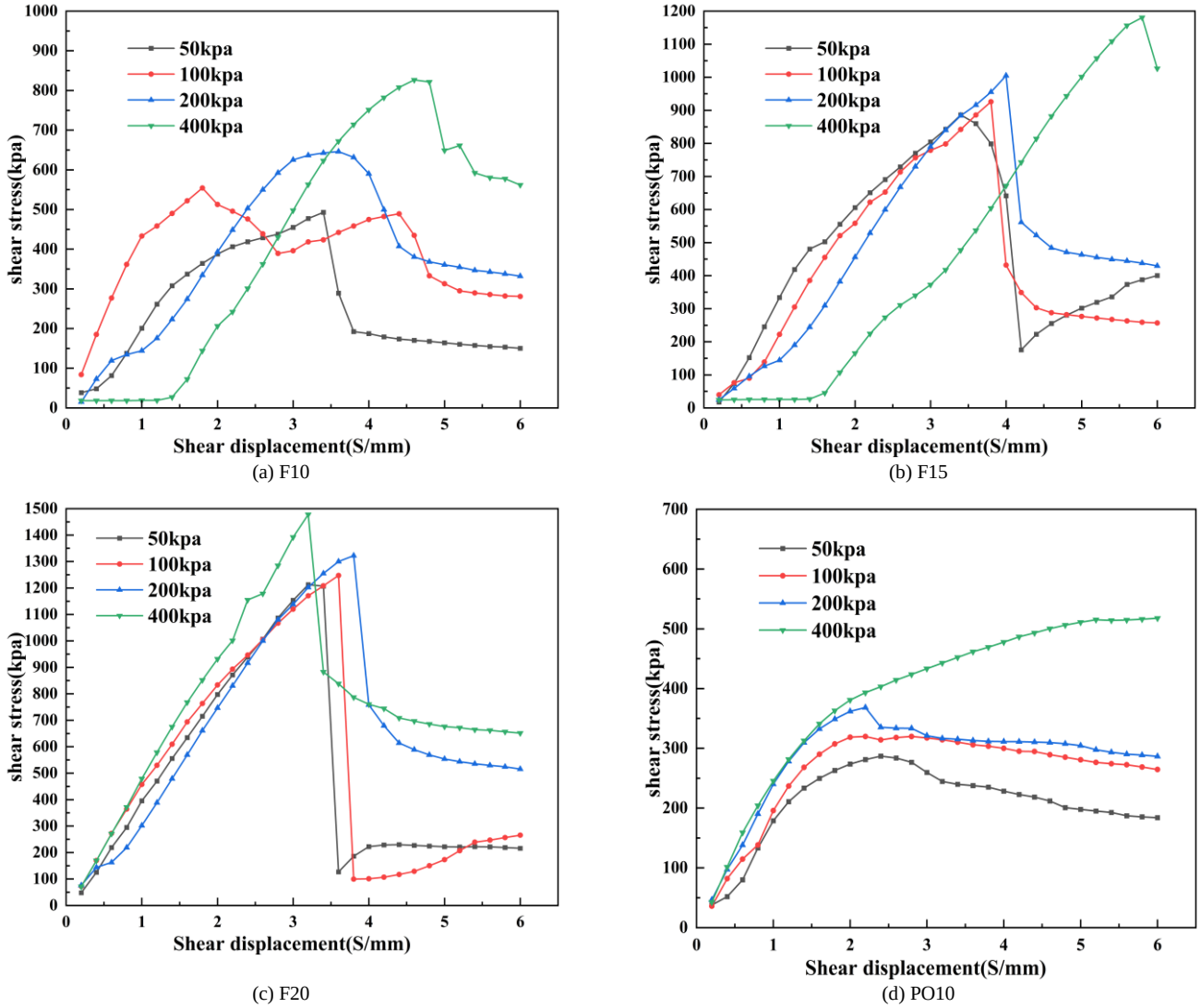

(a) F10 (b) F15

(c) F20 (d) PO10

Figure 4: Shear stress-strain curve for solidified calcareous silt at 14-day curing age (a)F10, (b)F15, (c)F20, (d)PO10

As illustrated in Figure 5, At the 28-day age, the solidified calcareous silt in the F group exhibited more pronounced brittle failure characteristics, with an increased number of failure curves displaying brittle fracture features. Furthermore, the quantity of these brittle failure curves followed a trend of 10% < 15% < 20% F content. The stress drop amplitude in the brittle failure curves increased significantly compared to earlier ages. Specifically, the 10% F group exhibited brittle failure curves under lower confining pressures (50 kPa and 100 kPa), whereas at the 14-day age, such curves were only observed at 50 kPa. At higher confining pressures, the 10% F group displayed brittle peak curves similar to those at the 7-day age, with peak values becoming flatter as the confining pressure increased. Meanwhile, the 15% and 20% F groups exhibited brittle peak curves and extremely significant brittle failures under higher confining pressures, respectively. These changes may be attributed to the ongoing hydration reactions with increasing age, which not only enhanced soil strength but also reduced the free water content, thus increasing soil brittleness [17]. Notably, the 20% As illustrated in Figure 5, group exhibited extremely significant brittle failures under all confining pressures, indicating a high degree of brittleness. The mechanical properties of the solidified calcareous silt in the cement group showed some similarity to those at the 7-day age. At lower confining pressures of 50 kPa and 100 kPa, the cement group exhibited brittle peak values similar to those of the 10% F group at the 7-day age. However, under higher confining pressures of 200 kPa and 400 kPa, the cement group displayed continuous and flat stress-strain curves, characteristic of plastic failure.

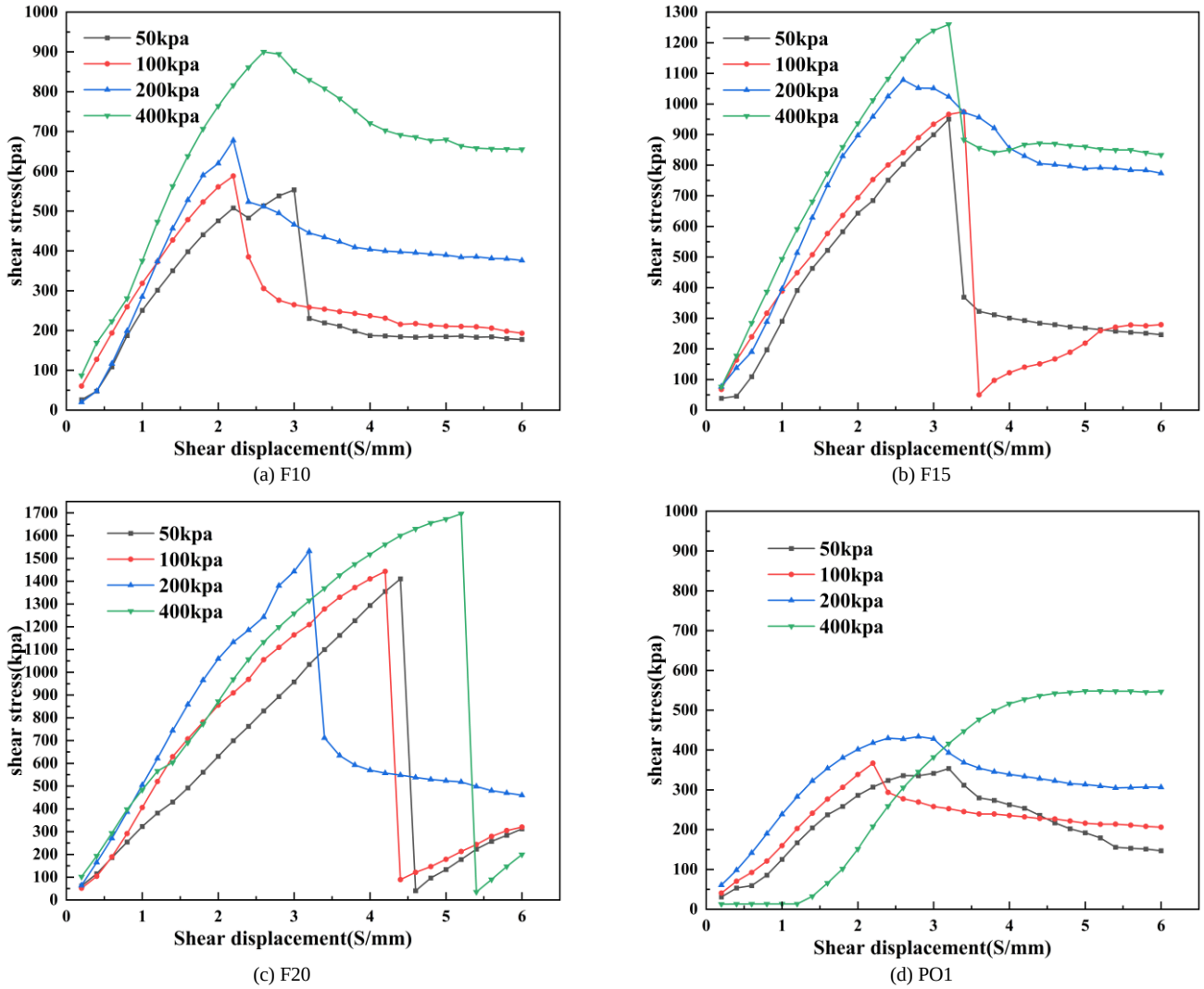

(a) F10 (b) F15

(c) F20 (d) PO1

Figure 5: Shear stress-strain curve for solidified calcareous silt at 28-day curing age (a)F10, (b)F15, (c)F20, (d)PO10

The failure mode and stress-strain relationship of the solidified calcareous silt in the F group were jointly influenced by F content, age, and confining pressure. With increasing age and ongoing hydration reactions, soil strength increased while free water content decreased. The cement group exhibited a relatively stable failure mode and stress-strain relationship over time. Compared to the F group, the stress-strain curves of the cement group were flatter. Both the cement and F groups exhibited an increase in brittleness.

3.2 Analysis of Experimental Results

Four different vertical pressures were applied to the solidified sludge samples, and the corresponding peak stresses under each vertical pressure were recorded. Linear fitting was performed between the shear strength values of the solidified sludge and the applied vertical pressures, followed by regression analysis of the linear fitting results. The coefficient of determination (R^2) for each linear fit was calculated. The R^2 values obtained from the linear fits were all greater than or equal to 0.989, indicating a high degree of goodness-of-fit. linear model accurately depicts the correlation between the shear resistance and the vertical stress of the solidified calcareous silt, as shown in Table 4.

Table 4: shear strength values

Types	Curing age	c	φ	R^2
PO	7d	214.09	32.86	0.985
PO	14d	250.14	33.3	0.993
PO	28d	318.35	29.77	0.995
F10	7d	403.31	39.9	0.998
F10	14d	453.95	43.2	0.998
F10	28d	491.76	45.11	0.994
F15	7d	785.64	39.08	0.989
F15	14d	841.55	40.1	0.999
F15	28d	895.35	42.27	0.996
F20	7d	1025.93	38.13	0.991
F20	14d	1172.41	37.27	0.999
F20	28d	1365.36	39.62	0.999

3.3 The Influence of Solidifier Dosage on Shear Performance

From the Figure 6, it can be observed that the ratio of cohesion c of the fluorogypsum group to cohesion c of the cement group, denoted as c(F)/c(PO), Exhibits a tendency to progressively diminish with aging and escalate with an increase in dosage level. The gradual decrease with age may be related to the large amount of fluorogypsum added in the fluorogypsum-based curing agent. During the initial stages of curing, fluorogypsum reacts with other components to generate a large amount of ettringite [18], effectively enhancing the strength of the solidified calcareous silt, resulting in a relatively high cohesion for the fluorogypsum

group in the early stages. As the age increases, cement gradually hydrates and demonstrates its advantage of having more cementitious components. In contrast, fluorogypsum - based curing agents contain relatively fewer cementitious components such as CSH and CASH [19], leading to a smaller increase in cohesion in the later stages and consequently a gradual decrease in the ratio of cohesion to that of cement.

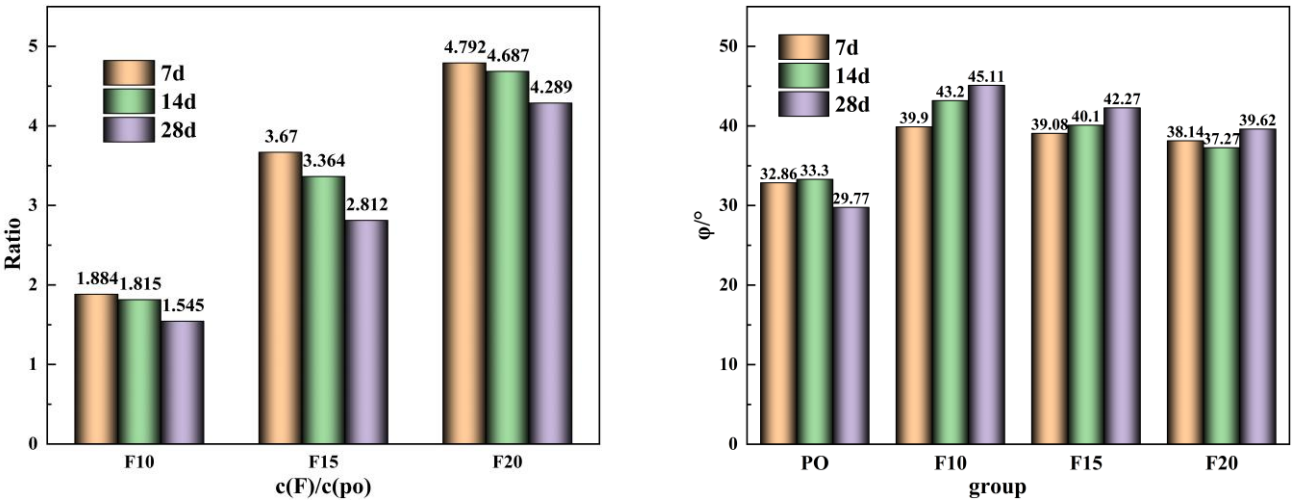

(a) Cohesion(F)/ Cohesion(PO) (b) φ

Figure 6: Variation rule of shear resistance with dosage

Analyzing the impact of dosage on cohesion, by subtracting the cohesion ratios of different dosages at the same age, we obtain F207d-F157d and F157d-F107d as 1.122 and 1.786, respectively; F2014d-F1514d and F1514d-F1014d as 1.323 and 1.549, respectively; and F2028d-F1528d and F1528d-F1028d as 1.477 and 1.267, respectively. It can be found that for the 7-day and 14-day ages, when the dosage increases from 10% to 15%, the proportion of cohesion for fluorogypsum-based solidified calcareous silt increases relatively significantly. This may be due to the fact that within this dosage range, the amount of ettringite produced in the solidified sludge is smaller, while the corresponding pores are relatively more abundant, and the reinforcing effect of ettringite is greater. When the dosage increases from 15% to 20%, the proportion increase for the 7-day and 14-day ages is smaller than that from 10% to 15%, but the increase for the 28-day age is greater than that from 10% to 15%. This may be because as the age increases, the consumption of calcium hydroxide in the system by hydration reactions increases. Fluorogypsum-based curing agents contain a large amount of slowly hydrated fly ash that requires sufficient alkalinity for hydration reactions [20]. A 20% dosage can better maintain the alkalinity of the system at the 28-day age, while 10% and 15% dosages suffer from insufficient alkalinity, resulting in a larger increase from 15% to 20% than from 10% to 15%.

Figure 6 reveals that the fluorogypsum group exhibits a higher internal friction angle than the cement group across all time points. The abundant ettringite formed during agent curing in fluorogypsum-Slag-Based group may be the reason. Ettringite acts as a micro-reinforcement [21] and simultaneously densifies the solidified calcareous silt, thereby enhancing φ of solidified calcareous silt. Except for the F group with a 20% dosage at the 7-day age, the internal friction angle gradually decreases with an increase in dosage. In contrast, the internal friction angle of the cement group exhibits a trend of first increasing and then decreasing.

3.4 The Influence of Curing Age on Shear Performance

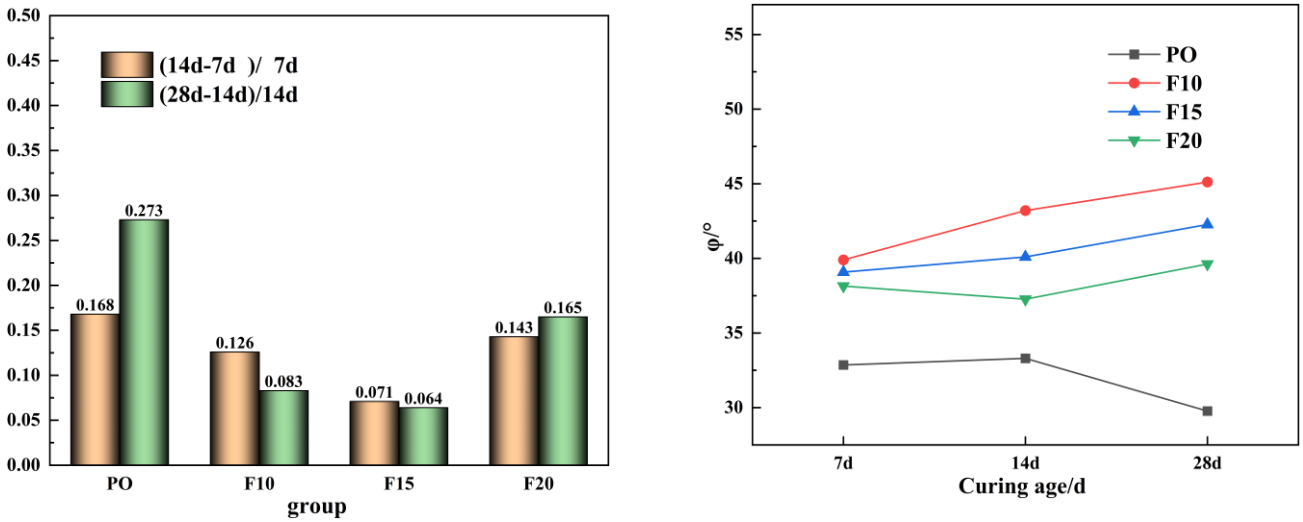

(a) Cohesion(bd)- Cohesion(ad)/ Cohesion(ad) (b) φ

Figure 7: Variation rule of shear resistance with curing age

Figure 7 indicates that the cohesion enhancement ratio of the F group is markedly lower than that of the cement group at any specified age. The maximum ratio for the F group is 0.165, which is less than the minimum ratio of 0.168 for the cement group. This indicates that the cohesion increment ratio of the cement group is greater than that of the F group at the same age. This is because the growth of cohesion depends on the formation of hydration products. During the nascent stages of hydration, ettringite can fill pores [22], increase the compactness of solidified sludge, and enhance its early strength. However, by the seventh day of hydration, the enhancing effect of ettringite formation diminishes, and the growth in shear strength primarily relies on the generation of gelatinous substances. The F group, due to the addition of some fluorogypsum, as well as slag and fly ash which hydrate more slowly, reduces the hydration rate. Meanwhile, the early enhancing effect of ettringite results in relatively high cohesion in the F group. In the later stages of hydration, the enhancing effect of hydration reactions is relatively small compared to the early enhancement of shear strength by ettringite, leading to a smaller increment ratio for the F group compared to the cement group.

The F group showcases a tendency of initial reduction succeeded by augmentation with regard to the doping level. This could be ascribed to the circumstance where the doping concentration rises from 10% to 15%, the amount of ettringite formed also increases. The early strength growth contributed by ettringite is higher than the strength growth attributed to gel-forming substances in later stages. As a result, higher initial cohesion values are observed. Therefore, there is a decrease in the cohesion increment ratio due to the increase in doping amount. When the doping amount increases from 15% to 20%, the corresponding alkalinity increases accordingly, and the gel-forming components also increase correspondingly. Consequently, the amount of gel-forming substances produced increases significantly. The strength growth contributed by these gel-forming substances becomes larger, leading to an increase in the cohesion increment ratio.

The increment ratio of cohesion for the cement group between the ages of 14 and 28 is much greater than that between 7 and 14 days. This is because as the age increases, the hydration reactions that were initially hindered due to insufficient alkalinity proceed normally. Meanwhile, it can be observed that for the fluorogypsum groups with doping amounts of 10% and 15%, The ratio of growth from the 7th to the 14th day surpasses that from the 14th to the 28th day. Similarly, for the 20% doping amount, the growth ratio between 7 and 14 days is also greater than that between 14 and 28 days. This may be due to the fact that during the 7 to 14-day period, ettringite in the fluorogypsum groups still exhibits a slight enhancing effect. Additionally, the cement components in the fluorogypsum, when sufficient alkalinity is present, can also play a significant role. However, the enhancement of solidified calcareous silt cohesion between 14 and 28 days is primarily attributed to the hydration reaction of slag and fly ash [23]. During the early stages, the formation of ettringite consumes a large amount of calcium hydroxide, resulting in a decrease in system alkalinity. For the fluorogypsum group with a 20% doping amount, during the 14 to 28-day period, a higher alkalinity is maintained. Simultaneously, the hydration of slag and fly ash produces a more dense geopolymer [24] cementitious material. Compared to the enhancement of shear strength contributed by cement components, the mechanical properties of geopolymer cementitious materials are superior. Therefore, for the F group, the growth ratio between 14 and 28 days is higher than that between 7 and 14 days.

The φ of the cement group demonstrates a pattern of initial augmentation succeeded by a diminution with age. In contrast, the F groups F10 and F15 show a gradual increase in internal friction angle with age, while F20 exhibits a pattern of initial decline followed by subsequent ascent. This may be attributed to the initial hydration stage where the cement group forms hydration products that fill pores, leading to an increase in φ. As the hydration process progresses, chemical shrinkage and physical deformation associated with cement hydration exert an influence on the internal friction angle, causing it to decrease.

4. Ultimate Bearing Capacity of Foundation

To investigate the disparities in engineering properties between cement-stabilized and fluorgypsum-based solidifier-stabilized calcareous silt, a foundation model was developed utilizing ABAQUS software. the ultimate bearing capacity of the foundation was computed when the stabilized calcareous silt served as the fill material.

4.1 Model Establishment and Parameters

The Mohr-Coulomb model can precisely captures the stress-strain behavior of solidified calcareous silt [25], Other models, such as HSS, have numerous parameters [26]. Therefore, the Mohr-Coulomb is chosen for numerical simulations of solidified calcareous silt. In consideration of the actual construction circumstances where loads are often imposed on the solidified silt foundation at an early age, the direct shear test data acquired at a 7-day curing duration was selected for simulation purposes. Based on a review of relevant literature [26] and considering the actual situation [20], parameters were adopted, as shown in the table below.

Considering the symmetry of the foundation model, half of the model is selected for analysis. A two-dimensional deformable solid with a side length of 7.5 meters is established, and the strip foundation with a width of 0.6 meters, half of it is taken for modeling. And a compressive load of 9 kPa is applied to the foundation surface. To ascertain the ultimate bearing capacity, a substantial displacement (0.3 m) is imposed on the strip foundation to ensure it attains the state of failure.

Table 5: The mechanical parameters of soil

Group	c/KPa	φ/°	E/ MPa	v	Ψ/°	Preload/KPa	γ/KN/m^3
PO10	214.09	32.86	20	0.3	0.1	9	18
F10	403.31	39.9	60				

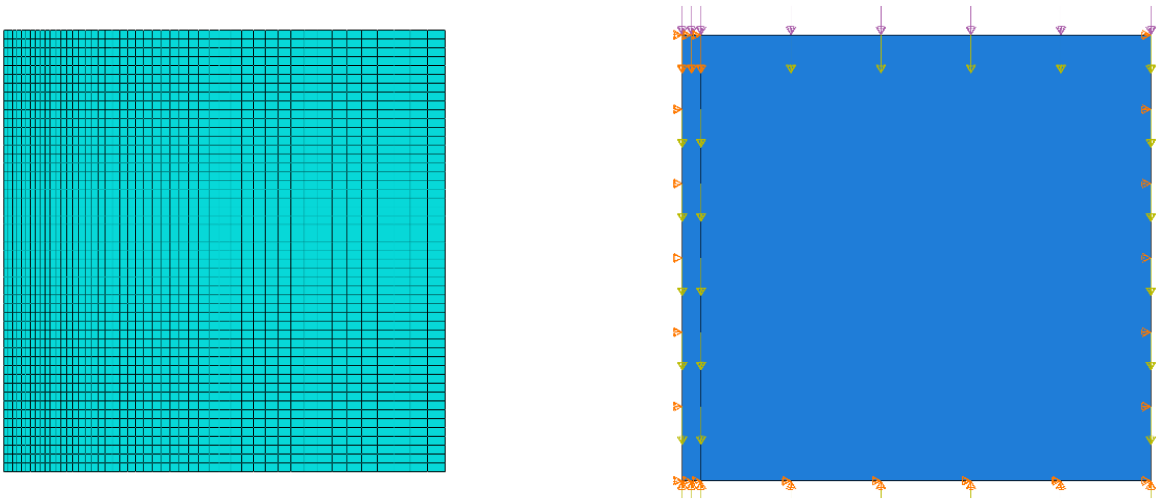

(a) mesh (b) load

Figure 8: Model

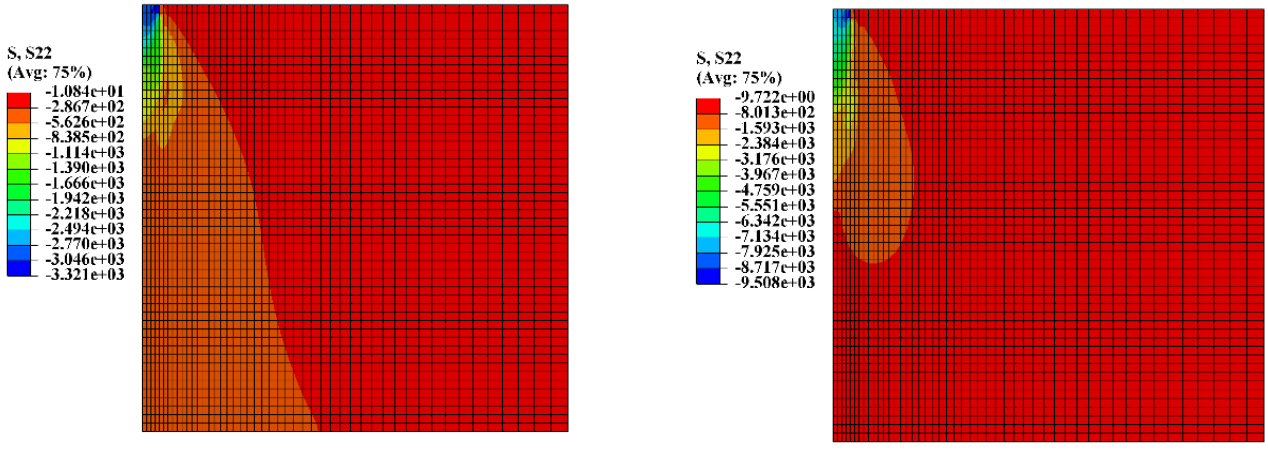

(a) PO10 (b) F10

Figure 9: Stress contour plot

4.2 Analysis of Numerical Simulation Results

The stress contour plot distinctly illustrates that the peak stress concentration occurs at the bottom edges of the loading plate of the strip foundation, constituting the area of maximum load within the entire foundation system. Furthermore, it is evident that the ultimate stress exhibited by the F10 group surpasses that of the cement group by a significant margin. The stress is localized in the vicinity of the strip foundation, whereas it diminishes significantly in regions distant from the strip foundation.

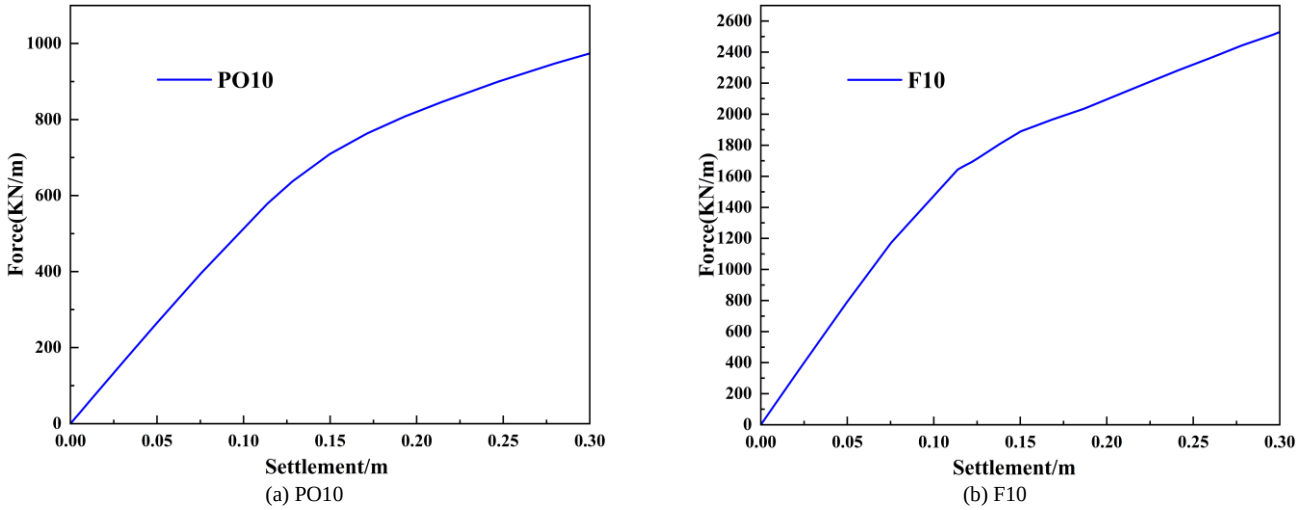

(a) PO10 (b) F10

Figure 10: Settlement Force Curve

Upon comparing the settlement-force curves of the PO10 and F10 groups, it is evident that the F10 curve exhibits superior mechanical properties and demonstrates more excellent engineering performance. By drawing tangents at both ends of

the two curves, the corresponding ultimate bearing capacities are obtained, which are 767.63 KN/m and 1638.225 KN/m for the PO10 and F10 groups, respectively. The corresponding ultimate bearing capacities of the foundation soil are calculated as 2558.8 KPa and 5460.75 KPa, respectively. It can be concluded that the fluorogypsum-based solidifier exhibits better engineering performance when used to solidify calcareous silt compared to cement-based solidification, as it can withstand greater loads.

5. Conclusion

(1) The stress-strain responses of calcareous silt stabilized with F agent and cement demonstrate notable disparities, with the fluorogypsum-treated group exhibiting a more pronounced slope and distinctive brittle failure traits in contrast to the cement-treated group. Under varying confining pressures, the failure characteristics of intra-group stress-strain curves diverge significantly, highlighting the substantial influence of confining pressure on the samples' stress-strain response.

(2) The cohesive strength of the F group increases with its content, however, an appropriate amount of ettringite filling is necessary, limited by the calcareous silt's pore structure. At 7-day and 14-day curing ages, the enhancement in cohesive strength ratio upon increasing content from 15% to 20% was less than 10% to 15%. However, at 28 days, the result was opposite to that at 7 and 14 days, as the 20% content provided sufficient alkalinity to maintain the hydration rate.

(3) Due to the hydration reaction, free water is converted into bound water, and calcium hydroxide is continuously produced, leading to a significant increase in the strength of the cement group between 14 and 28 days of age. In the F group, the strength was already relatively high before 7 days, and the increase in cohesive strength caused by the gelatinous substances in the later stages was relatively small.

(4) Numerical simulations conducted using Abaqus indicate that the fluorogypsum-based stabilizer significantly outperforms the cement-based counterpart in solidifying calcareous silt foundations, demonstrating enhanced shear strength and elevated ultimate bearing capacity. The stress contour plots of the solidified silt reveal that the maximum stress is concentrated at the bottom corners of the strip foundation's loading plate, with a decreasing stress gradient observed as the distance from the loading point increases.

References

[1] K. Hamer and V. Karius, "Brick production with dredged harbour sediments. An industrial-scale experiment," *Waste Management*, vol. 22, no. 5, pp. 521–530, Aug. 2002, doi: 10.1016/ s0956-053x (01)00048-4.

[2] D. Wang, N. E. Abriak, and R. Zentar, "Dredged marine sediments used as novel supply of filling materials for road construction," *Marine Georesources & Geotechnology*, vol. 35, no. 4, pp. 472–480, May 2017, doi: 10.1080/1064119x.2016.1198945.

[3] B. Lucke and U. Schmidt, "Grain size analysis of calcareous soils and sediments: inter- method comparison with and without calcium carbonate removal".

[4] S.-Y. Pu, Z.-D. Zhu, W.-L. Song, H.-R. Wang, and R.-J. Wei, "Deformation properties of silt solidified with a new SEU-2 binder," *Construction and Building Materials*, vol. 220, pp. 267–277, Sep. 2019, doi: 10.1016/j.conbuildmat.2019.06.016.

[5] S. Pu, Z. Zhu, H. Wang, W. Song, and R. Wei, "Mechanical characteristics and water stability of silt solidified by incorporating lime, lime and cement mixture, and SEU-2 binder," *Construction and Building Materials*, vol. 214, pp. 111–120, Jul. 2019, doi: 10.1016/j.conbuildmat.2019.04.103.

[6] M. Yousuf, A. Mollah, J. R. Pargat, and D. L. Cocke, "An infrared spectroscopic examination of cement-based solidification/stabilization systems - Portland types V and IP with zinc," *Journal of Environmental Science and Health. Part A: Environmental Science and Engineering and Toxicology*, vol. 27, no. 6, pp. 1503–1519, Aug. 1992, doi: 10.1080/10934529209375809.

[7] D. A. Salas, A. D. Ramirez, C. R. Rodríguez, D. M. Petroche, A. J. Boero, and J. Duque-Rivera, "Environmental impacts, life cycle assessment and potential improvement measures for cement production: a literature review," *Journal of Cleaner Production*, vol. 113, pp. 114–122, Feb. 2016, doi: 10.1016/j.jclepro. 2015.11.078.

[8] Li et al. Strength characteristics and solidification carbon.pdf."

[9] J. Xiao, J. Shen, M. Bai, Q. Gao, and Y. Wu, "Reuse of construction spoil in China: Current status and future opportunities," *Journal of Cleaner Production*, vol. 290, p. 125742, Mar. 2021, doi: 10.1016/ j.jclepro. 2020.125742.

[10] L. Bayatanova et al., "Production of Anhydrite Binder from Waste Fluorangydrite," *ChemEngineering*, vol. 7, no. 2, p. 28, Mar. 2023, doi: 10.3390/ chemengineering 7020028.

[11] A. A. B. Moghal, "State-of-the-Art Review on the Role of Fly Ashes in Geotechnical and Geoenvironmental Applications," *J. Mater. Civ. Eng.*, vol. 29, no. 8, p. 04017072, Aug. 2017, doi: 10.1061/ (ASCE)MT. 1943-5533.0001897.

[12] K. S. Rodygin, Y. A. Vikenteva, and V. P. Ananikov, "Calcium-Based Sustainable Chemical Technologies for Total Carbon Recycling," *ChemSusChem*, vol. 12, no. 8, pp. 1483–1516, Apr. 2019, doi: 10.1002/ cssc. 201802412.

[13] C. Pan, X. Xie, J. Gen, and W. Wang, "Effect of stabilization/solidification on mechanical and phase characteristics of organic river silt by a stabilizer," *Construction and Building Materials*, vol. 236, p. 117538, Mar. 2020, doi: 10.1016/ j.conbuildmat. 2019.117538.

[14] Y. Wang, Z. Wang, Y. Chen, T. Cao, X. Yu, and P. Rui, "Experimental study on bio-treatment effect of the dredged Yellow River silt based on soybean urease induced calcium carbonate precipitation," *Journal of Building Engineering*, vol. 75, p. 106943, Sep. 2023, doi: 10.1016/j.jobe.2023.106943.

[15] W. Hou et al., "Experimental study on the strength characteristics and seawater degradation resistance of sandy silt solidified with alkali-activated slag,"

Construction and Building Materials, vol. 458, p. 139610, Jan. 2025, doi: 10.1016/ j.conbuildmat. 2024. 139610.

[16] H. F. W. Taylor, C. Famy, and K. L. Scrivener, "Delayed ettringite formation$," *Cement and Concrete Research*, 2001.

[17] A. Behnood, "Soil and clay stabilization with calcium- and non-calcium-based additives: A state-of-the-art review of challenges, approaches and techniques," *Transportation Geotechnics*, vol. 17, pp. 14–32, Dec. 2018, doi: 10.1016/j.trgeo.2018.08.002.

[18] M. Chrysochoou and D. Dermatas, "Evaluation of ettringite and hydrocalumite formation for heavy metal immobilization: Literature review and experimental study," *Journal of Hazardous Materials*, vol. 136, no. 1, pp. 20–33, Aug. 2006, doi: 10.1016/j.jhazmat. 2005.11.008.

[19] C. Roosz et al., "Thermodynamic properties of C-S-H, C-A-S-H and M-S-H phases: Results from direct measurements and predictive modelling," *Applied Geochemistry*, vol. 92, pp. 140–156, May 2018, doi: 10.1016/j.apgeochem.2018.03.004.

[20] I. Wilińska and B. Pacewska, "Comparative investigation of reactivity of different kinds of fly ash in alkaline media," *J Therm Anal Calorim*, vol. 138, no. 6, pp. 3857–3872, Dec. 2019, doi: 10.1007/ s10973-019-08296-4.

[21] Q. Wang, Y. Yi, G. Ma, and H. Luo, "Hybrid effects of steel fibers, basalt fibers and calcium sulfate on mechanical performance of PVA-ECC containing high-volume fly ash," *Cement and Concrete Composites*, vol. 97, pp. 357–368, Mar. 2019, doi: 10.1016/j.cemconcomp.2019.01.009.

[22] Y. Gu, R.-P. Martin, O. Omikrine Metalssi, T. Fen-Chong, and P. Dangla, "Pore size analyses of cement paste exposed to external sulfate attack and delayed ettringite formation," *Cement and Concrete Research*, vol. 123, p. 105766, Sep. 2019, doi: 10.1016/j.cemconres.2019.05.011.

[23] M. Albitar, M. S. Mohamed Ali, P. Visintin, and M. Drechsler, "Effect of granulated lead smelter slag on strength of fly ash-based geopolymer concrete," *Construction and Building Materials*, vol. 83, pp. 128–135, May 2015, doi: 10.1016/j.conbuildmat. 2015.03.009.

[24] N. Hui-Teng, H. Cheng-Yong, M. M. A. B. Abdullah, N. Yong-Sing, and R. Bayuaji, "STUDY OF FLY ASH GEOPOLYMER AND FLY ASH/SLAG GEOPOLYMER IN TERM OF PHYSICAL AND MECHANICAL PROPERTIES," *EJMSE*, vol. 5, no. 4, pp. 187–198, Dec. 2020, doi: 10.36868/ejmse. 2020.05.04.187.

[25] S. Li, Y. Lai, S. Zhang, and D. Liu, "An improved statistical damage constitutive model for warm frozen clay based on Mohr–Coulomb criterion," *Cold Regions Science and Technology*, vol. 57, no. 2–3, pp. 154–159, Jul. 2009, doi: 10.1016/j.coldregions.2009.02.010.

[26] J. Kwon, X. Wang, F. Blaabjerg, C. L. Bak, V.-S. Sularea, and C. Busca, "Harmonic Interaction Analysis in a Grid-Connected Converter Using Harmonic State-Space (HSS) Modeling," *IEEE Trans. Power Electron.*, vol. 32, no. 9, pp. 6823–6835, Sep. 2017, doi: 10.1109/TPEL.2016.2625802.